Investigation of the compression dynamics in gas-filled microspheres with aspect ratio $R/\Delta R = 30$–300 in experiments on the "SOKOL" facility

M. G. Anuchin, V. V. Volenko, A. I. Zuev, A. F. Ivanov, V. A. Lykov, L. A. Myalitsin, L. A. Osadchuk, and A. I. Saukov

(Submitted 14 April 1987)
Zh. Eksp. Teor. Fiz. **94**, 25–39 (May 1988)

An interpretation is presented of the results of research into the gasdynamic parameters and the compression dynamics of gas-filled microspheres with $R/\Delta R = 30$–300, obtained with the "SOKOL" facility at incident and absorbed laser energy flux densities $q \approx (0.1\text{–}4.0)\cdot 10^{14}$ W/cm^2 and $q_a \approx (0.1\text{–}1.0)\cdot 10^{14}$ W/cm^2 and at specific energy inputs $\varepsilon_0 \approx 0.003$–$0.3$ J/ng. The dependences of the average flight velocity of the shell towards the center, of the average scatter rate of the laser plasma, of the mass flow rate, of the average ablation pressure, of the hydrodynamic efficiency, and of the mass coefficient on the indicated physical parameters are investigated. The results are used to reconcile and optimize the parameters of the laser + target system so as to increase the specific energy input. The heat-conduction confinement coefficient is obtained in greater detail by comparison of the experimental results with those of gasdynamic calculations. It is concluded that the electronic heat flux is weakly confined under the conditions of the experiments with the "SOKOL" facility. The results are compared with those of theoretical models, with gasdynamic calculations, and with data obtained with the "Kal'mar," "Delphin," "Vulkan," "Chroma-I," "Omega," and the "Argus" facilities.

INTRODUCTION

At contemporary levels of laser energy, of target manufacture precision, and of target-irradiation symmetry, experimental investigations of the hydrodynamic processes of the target expansion and contraction, of the DT-gas heating, and of neutron generation are the central problems in experiments on laser-driven thermonuclear fusion.[1–4] The investigation of target-compression dynamics can be regarded as an essential part of the general gasdynamic problem. The main purpose at this stage is the measurement of such laser-plasma gasdynamic parameters and of their physical properties which optimize the laser + target system and permit also a refinement and calibration of the physical models and gasdynamic-computation programs on the basis of which one can formulate the requirements that must be met by the parameters of the targets and of the high-power laser systems needed to reach the physical thermonuclear-fusion threshold.

We report here the results of an investigation of the dynamics of compression of gas-filled glass microspheres in experiments with the "SOKOL" facility,[5,6] carried out during the operation of this facility (1976–1984). The parameters were the following: the laser energy focused on the critical target dimension $2R_{cr} \approx 10$–150 μm was $E_l \approx 100$–170 J and 50–70 J at pulse durations (widths at half-maximum) $\tau_p = 1.0$ and 0.3 ns, corresponding to target flux densities $q = E_l/4\pi \overline{R}_{cr}^2 \tau_p$ $q \approx 2\cdot 10^{14}$ and $q \approx 4\cdot 10^{14}$ W/cm^2, respectively. The measured laser parameters were: shell diameter $2R_t \approx 140$–190 μm, shell thickness $\Delta R \approx 0.8$–1.5 μm, and DT gas pressure $P_{DT} \approx 5$–25 atm for an aspect ratio $R/R = 30$–80, and $2R_t \approx 140$–180 μm, $\Delta R \approx 0.3 = 0.6$ μm, and $P_{DT} \approx 1$–10 atm for $R/\Delta R = 100$–300.

1. OPTIMIZATION OF THE LASER + TARGET SYSTEM PARAMETERS

In laser experiments, the parameter that determines the strength of the DT-gas compression and heating is the specific input reached by the instant of maximum compression

$$\varepsilon_0 = \frac{1}{M_0}\int_0^{\tau_*} \dot{E}_n(t)\,dt,$$

where M_0 is the initial target mass, $\dot{E}_n t$ is the absorbed laser energy, and τ_* is the target collapse time. Analytic scaling,[8–10] confirmed by gasdynamic calculations, shows that the degree of compression and the DT-gas temperature under adiabatic compression are increasing function of the specific energy input:

$$\delta \propto (\varepsilon_0'\Delta R/\rho_{DT_0}R_M)^{1/(\gamma-1)},$$
$$T_{DT}{}^i \propto \varepsilon_0'/\rho_{DT}{}^0, \qquad (1)$$

where $\varepsilon_0' = E_{comp}/M_{comp}$ is the ratio of the energy of the compressed part of the target to its mass, and ρ_{DT}^0 is the initial DT gas density. The relation between ε_0 and ε_0' is $\varepsilon_0' = \varepsilon_0\,\eta_h/\eta_t$, where the coefficient of the hydrodynamic energy transfer of the compressing part of the target (the hydrodynamic efficiency)

$$\eta_h = E_{comp}\Big/\int_0^{\tau_*}\dot{E}_n(t)\,dt$$

and the mass coefficient $\varepsilon_t = M_{comp}/M_0$ are slowly varying functions of the specific energy input. The maximum shell flight velocity towards the center v_{max} and the neutron yield N_{DT} are also functions of the specific energy input, which enters in N_{DT} via the degree of compression and the temperature of the DT gas:

$$v_{max} = (2\varepsilon_0')^{1/2}, \quad N_{DT} \approx 1.5\cdot 10^{18}\left(\frac{M_{DT}}{R_M}\right)^2 \delta^{7/3} T_i^{\alpha}, \qquad (2)$$

where $[M_{DT}]$ is in grams, $[T_i]$ in keV, $[R_t]$ in cm, and M_{DT} is the DT-gas mass.

An increase of the specific heat input leads thus to an increase of the temperature and of the density of the DT gas, and hence to a growth of the neutron yield. This conclusion is the basis for optimizing the parameters of the laser + target system. Thus, the parameters of the target and of the laser pulse must be reconciled in the course of the optimiz-

 0038-5646/88/050880-09$04.00

ation in such a way that the instant of target collapse occurs when the action of the laser pulse terminates, and the specific energy input ε_0 increases in this case. This, in turn, requires knowledge of the dependence of the laser-energy absorption coefficient on the flux density,[11] and measurements of the gasdynamic parameters, viz., the target collapse time τ_*, the average ($\bar{v}$) and maximum (v_{max}) velocities of the shell motion towards the center, the specific energy input ε_0, the R-t diagrams of the characteristic regions of the laser plasma, the time profile of the x-ray power $P_x(t)$, and others. It must be noted that this approach to optimization is applicable mainly to isentropic target compression, when $q\lambda^2 < 10^{15}$ W/cm^2/μm^{-2} and $\tau_p \approx \tau_*$, and is universal in a wide range of specific energy inputs and aspect ratios.

2. INVESTIGATION OF THE DYNAMICS OF COMPRESSION OF GAS-FILLED GLASS MICROSPHERES

The expansion and compression dynamics was investigated in the "SOKOL" facility by the following diagnostic procedures:

1. "Shock wave"—measurement of the absorbed energy E_a by recording the $R(t)$ dependences of the shock wave propagating in the residual gas surrounding the target, using multiframe ultrahigh-speed shadow and Schlieren photography.[6,12]

2. "Ions"—measurement of the absorbed energy and of the energy makeup of the laser plasma ions by on collectors.[12]

3. "Corona"—investigation of the behavior, in space and in time, of the target image in the light of the second harmonic, and measurement of $R_{cr}(t)$ dependence of the target corona.[13]

4. "TXD"—measurement of the temporal profile of the x-ray spectral intensity. The measurements were made with a vacuum x-ray diode quite similar to that described in Ref. 14, but with an aluminum cathode. The use of an x-ray filter ($0.6\,\mu$m Al + $10\,\mu$m $(CH_2)_n$) set the photon energy range at $h\nu \approx 1.5$–40 keV, corresponding to the x-ray emission from the corona of the laser plasma (contained between the evaporation front and the critical-density limit) and corresponding to the registration range of the integral x-ray photographs of the irradiated target.[16] The temporal profile of the x-ray pulse was recorded by SRG-5 and S7-15 oscilloscopes for x-ray diodes with wave resistances 75 and 50 Ω, respectively. The time resolution of the method is $\approx$0.2–0.3 ns, and the calculated sensitivity of the diode at the maximum is $S_{max} \approx 8 \cdot 10^{-22}$ K/keV, $(h\nu)_{max} \approx 2.2$ keV.

5. "Lines"—measurement of the x-ray line spectrum in an energy range $\approx$1–3 keV. The method is based on photography of the x-ray lines of multiply charged ions separated by crystal spectrometers.[17]

6. "Pulse"—registration of time profile of the laser pulse. The method is implemented in two variants—oscillographic and electron-optical. In the first variant the pulse profile was recorded by an FÉK-15KP coaxial photocell with a rated resolution $\approx$0.1 ns. The photocell was connected by an RK75-9-12 cable 1–2 m long to an SRG-5 high-speed oscilloscope capable of recording a front with a rise time $\approx$0.2 ns. For more detailed time measurements we used an image converter based on an LV-03 "time magnifier" operating in the slit-scanning regime. The image converter was controlled by a high-voltage pulse shaped by a laser-ignited discharge gap, ensuring a scanning rate $\approx$2–3 mm/ns over the screen and a time resolution $\approx$0.05 ns.

Gasdynamic calculations using the "Zarya" program[18] show (see Fig. 1) that the $R(t)$ dependence of the corona region with critical density reaches a minimum at instants of time close to the target-collapse instant. The power $P_x(t)$ of the x rays emitted by the target has in this case a sharp maximum due to the conversion of the kinetic energy of the contracting part of the target into internal energy of the plasma. The subsequent expansion leads to an abrupt decrease of the x-ray intensity. By recording the time dependences of R_{cr} and R_x it is thus possible to measure the target-collapse time, the average velocity v of the shell travel towards the center, and the specific energy input ε_0.

Figure 1 shows also typical experimental $R(t)$ dependences of the region of the critical-density corona, measured in experiments Nos. 33 and 63, where $\tau_* > \tau_p^0$ and $\tau_* < \tau_p^0$, respectively ($\tau_p^0 \approx 1.3$ ns is the duration of the laser pulse at the base). It can be seen that the collapse times determined by measuring $R_{cr}(t)$ and by calculation are equal within the limits of error for experiment No. 63. The experimental and calculated R_{cr} dependences agree sufficiently well with one another, a situation typical of flux densities $q < (2\text{–}3) \cdot 10^{14}$ W/cm^2.

On the other hand, at fluxes $q \gtrsim (2\text{–}3) \cdot 10^{14}$ W/cm^2, modulation with a period $\tau_m \approx$0.4–0.5 ns is observed, both in the critical dimension $R_{cr}(t)$ of the target corona and in the intensity of the $2\omega_0$ harmonic generation. In this case the measured and calculated $R_{cr}(t)$ dependences differ noticeably in the region $t \approx$0.2–0.8 ns. This is due to the action of the ponderomotive pressure $\mathbf{F} = (1-\varepsilon)\nabla E_*^2/4\pi\varepsilon^{1/2}$ (ε is the plasma dielectric constant) of the laser radiation in the region of the critical density,[19–21] which is not taken into account in the "Zarya" gasdynamic program. Calculations[20–22] with account taken of the laser-radiation pressure show that in the critical region a jump takes place in the

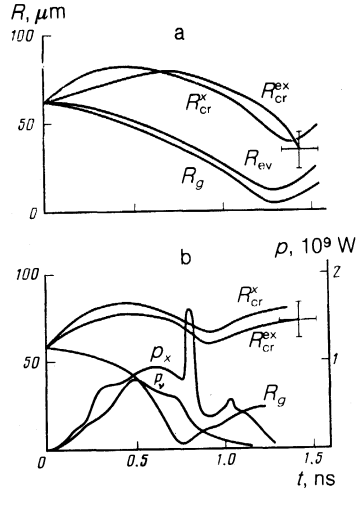

FIG. 1. Time dependences $R(t)$ of the corona region R_{cr} with critical density (experiment and calculation), of the evaporation boundary R_{ev}, of the interface R_g between the DT gas and the glass (calculation), the time profile $P_x(t)$ of the power (calculated) and $P_v(t)$ of the spectral intensity (experiment, relative units), of the x radiationL a—experiment No. 33, $2R_i \approx 121.4\,\mu$m, $\Delta R \approx 1.5\,\mu$m, $P_{DT} \approx 10$ atm, $\tau_p \approx 1.1$ ns, $E_a \approx 11.7$ J, $q \approx 1.5 \cdot 10^{14}$ W/cm^2; b—experiment No. 63, $2R_i \approx 114\,\mu$m, $\Delta R \approx 0.8\,\mu$m, $P_{DT} \approx 12$ atm, $\tau_p \approx 1.0$ ns, $E_a \approx 15.4$ J, $q \approx 1.1 \cdot 10^{14}$ W/cm^2.

density profile; in the case of subsonic flow of the substance, a dip ("caviton") is produced in the critical region and remains stable there; if the flow is supersonic, however, as is usual in laser experiments,[10,12] a caviton is produced, but is carried out by the ponderomotive forces into less dense regions and spreads out, after which a following caviton is produced, and it is this which leads to modulation of $R_{cr}(t)$. Measurement of the modulation period τ_m, of the $R_{cr}(t)$ dependence, and of the average energy $\langle \varepsilon_e^{\sigma} \rangle$ of the laser plasma fast electrons yields estimates of the electric field E_* and of the characteristic scale L_{E_*} of its change in the critical region:

$$E_* = (4\pi\rho_{cr})^{1/2} R_{cr}/3\tau_t, \quad L_{E_*} = 2\langle \varepsilon_e^6 \rangle / eE_*, \qquad (3)$$

where e is the electron charge and $\rho_{cr} \approx 3.5 \times 10^{-3}$ g/cm^3. Under the operating conditions of the "SOKOL" facility, $E_* = 10^8$ V/cm and $L_{E_*} \approx 0.3$–0.7 μm. This points to the presence of a density profile jump in the critical region, and confirms the conclusions of Ref. 11.

It should be noticed furthermore that the "Corona" procedure permits measurement of the collapse time only if the target collapse occurs during the time of action of the laser pulse, i.e., when radiation of frequency $2\omega_0$ is generated. In the "TXD" procedure, however, one can in principle measure τ_* also when the collapse is produced after the end of the action of the laser pulse. This is important for the investigation of the effect of asymmetry on the compression dynamics. We also measured with the "SOKOL" facility the time dependence of laser-radiation power $P_{2\alpha}(t)$ focused in a solid angle $2\alpha \approx 4 \cdot 10^{-4}$ rad. In conjunction with the experimental dependence of the geometric interaction factor f_g on the radius R_{cr} this makes it possible to find the time dependence of the laser radiation power $P_0(t)$ incident on the target and the instantaneous volume of the laser-energy flux density $q(t) = P_0(t)/4\pi R_{cr}^2(t)$ on the target.

The x-ray spectral-intensity time profiles $P_*(t)$ measured in experiments 63, 64, and 84 are shown in Figs. 1b and 2, respectively. The figures show also the calculation results for experiment No. 63 and the results of other temporal measurements. The experimental $P_\nu(t)$ plots do not show the sharp and tall peak due to the target collapse and deduced from gasdynamic calculations. The main reason for this difference lies in the instrumental function, which characterizes the time resolution of the "TXD" method and broadens the short-time spikes and lowers their amplitude.[13] In addition, the deviations from one-dimensionality in the experiments causes the motion and shell collapse to deviate from spherical symmetry and lowers the intensity of the x-ray emission during the collapse. A comparative analysis of the results of the temporal measurements shows that the instant of the x-ray intensity maximum $P_\nu(t)$ agrees within the limits of error with the moment when the instantaneous value of the flux density $q(t)$ at the target also reaches a maximum. The latter corresponds in turn, if $\tau_* \ll \tau_p$, to the instant of the maximum of the $R_{cr}(t)$ dependence. The reason is that the plasma electron temperature in the target corona is $T_e \propto q^{2/7}$ (Ref. 23), i.e., the maximum flux density $q(t)$ corresponds to the highest value of the temperature T_c and hence to the maximum emissivity of the plasma and x-ray energy flux density $S_\nu(t)$. On the other hand, the connection $P_\nu(t) \propto S_\nu(t) R_{cr}^2(t)$ between the spectral intensity $P_\nu(t)$ of the x rays with the flux $S_\nu(t)$ explains the insignificant time shift (≈ 10 ps) of the maximum of $P_\nu(t)$ at large radii $R_{cr}(t)$ relative to the time max $q(t)$. In this case the values of the collapse time τ_* obtained from min $R_{cr}(t)$ and from max $P_\nu(t)$ are equal within the limit of experimental error. If, however, the target collapse occurs either on the trailing edge of the laser pulse, or else $\tau_* \approx \tau_p^0$, the instant max $q(t)$ corresponds to the start of the laser-pulse fall-off and differs substantially ($\gtrsim 0.3$ ns) from the real instant of target collapse, see Fig. 2b.

Figure 3 shows the measured forms of the x-ray pulse in the case when the collapse time definitely exceeds the laser-pulse duration, $\tau_* > \tau_p^0$, for experiments No. 56, 76, and 77. In similar experiments one observes as a rule, after termination of the laser pulse, a second x-ray intensity maximum corresponding to the target collapse. This is confirmed by a collapse-time estimate based on the $\bar{v} = R_t/\tau_* = f(\varepsilon_0)$ dependence measured with the SOKOL facility.

The main laws governing the time dependences of the x-ray intensity in the soft region $h\nu \lesssim 0.3$ keV, measured with open (without a filter) "TXD," agree with those of Ref. 14, where it was shown that the x-ray pulse trailing edge, which is protracted in this case, is due to recombination and photon line emission from a nonequilibrium plasma under conditions of "quenching" of the ionization state.

Systematic measurements of the dynamics of the compression of glass-filled microspheres, carried out in the experiments with the "SOKOL" facility, have made it possible to investigate the dependence of the average velocity of the

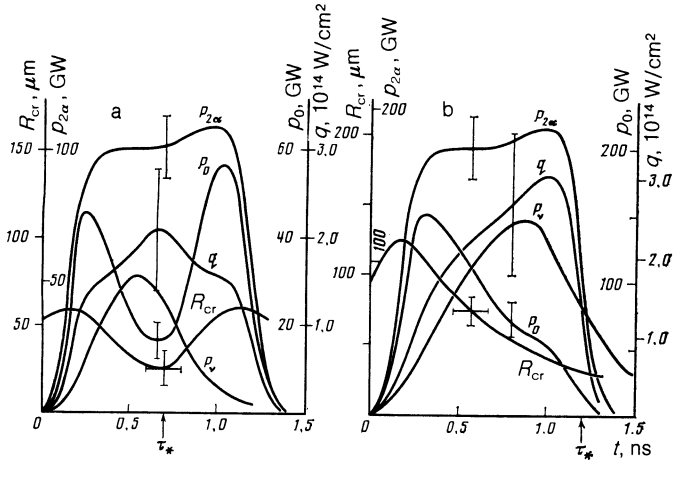

FIG. 2. Measured time dependences of $R_{cr}(t)$, $P_{2\alpha}(t)$, $P_0(t)$, $q(t)$ and $P_\nu(t)$: a—experiment No. 64, 14 atm, $\tau_p \approx 1.0$ ns, $E_a \approx 11.9$ J, $q \approx 1.7 \cdot 10^{14}$ W/cm^2; b—experiment No. 84, $2R_t \approx 187.2$ μm, $\Delta R \approx 0.5$ μm, $P_{DT} \approx 7$ atm, $\tau_p \approx 1.0$ ns, $E_a \approx 26.8$ J, $q \approx 1.5 \cdot 10^{14}$ W/cm^2.

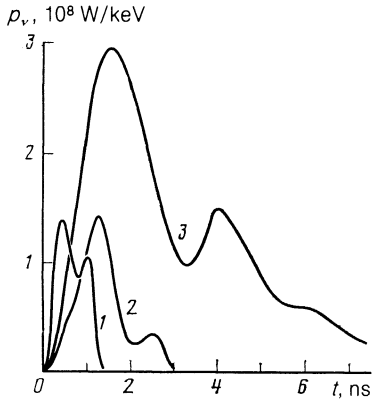

FIG. 3. Time profile of x-ray spectral intensity in the case $\tau_* > \tau_p^0$: 1—experiment No. 56, $2R_i \approx 142.6$ μm, $\Delta R \approx 0.3$ μm, $P_{DT} \approx 1$–3 atm, $\tau_p \approx 0.3$ ns, $E_a \approx 5.3$ J, $q \approx 2.7 \cdot 10^{14}$ W/cm^2; 2—experiment No. 76, $2R_i \approx 307.3$ μm, $\Delta R \approx 4.7$ μm, $P_{DT} \approx 0$, $\tau_p \approx 2.5$ ns, $E_a \approx 125$ J, $q \approx 0.3 \cdot 10^{14}$ W/cm^2; 3—experiment No. 77, $2R_i \approx 320$ μm, $\Delta R \approx 2.7$ μm, $P_{DT} \approx 0$, $\tau_p \approx 1.0$ ns, $E_a \approx 95$ J, $q \approx 0.65 \cdot 10^{14}$ W/cm^2; $\overline{h\nu} \approx 1.9 \binom{+1.9}{-0.4}$ keV.

shell travel towards the center on the specific energy input, on the absorbed-energy flux density $q_a = E_a/4\pi \overline{R}_{cr}^2 \tau_p$, and on the aspect ratio; see Figs. 4 and 5. The relations obtained agree with the results of Refs. 24–26 and are well interpolated by the relations

$$\bar{v} = 1.6 \cdot 10^7 \varepsilon_0^{1/2} \text{ cm/s},$$
$$\bar{v} = 0.17 \cdot 10^7 q_a^{1/3} (R/\Delta R)^{0.4} \text{ cm/s}, \quad [q_a] = 10^{14} \text{ W/cm}^2, \tag{4}$$

which accord with the scaling relations that follow from the theoretical models[10,22,23]:

$$P_a \approx 0.28 q_a^{2/3} \rho_{cr}^{1/3},$$
$$\bar{v} = \left(\frac{P_a}{6\eta_m \rho} \frac{R}{\Delta R}\right)^{1/2} = \text{const}\, q_a^{1/3} \left(\frac{R}{\Delta R}\right)^{1/2} \eta_m^{-1/2}$$
$$= \text{const}' \varepsilon_0^{1/2} \left(\frac{R}{\Delta R}\right)^{1/4} \eta_m^{-3/4}, \tag{5}$$

where P_a is the ablation pressure. The straight lines in Figs. 4 and 5 were drawn through the experimental results by least squares, and correspond to relations (4). The rather good agreement between the experimental and theoretical dependences of the average velocity $\bar{v}$ on the specific energy input ε_0, on the absorbed laser energy flux density q_a, and on the aspect ratio $R/\Delta R$ identifies the target and laser-pulse principal parameters that determine the compression dynamics in the experiments and corroborates the approach proposed in this paper to the optimization of the laser + target system.

Our comprehensive measurements of the dynamic compression parameters and their comparative analysis have thus made it possible to determine the gasdynamic parameters τ_*, $\bar{v}$, and ε_0, to measure the alternating component of the electron temperature in the target corona,[13] to assess the sphericity of the target compression, and to optimize the target and laser-pulse parameter in accord with the criterion formulated in Sec. 1. A similar optimization was carried out in experiments with the "SOKOL" facility and made it possible to reach, for targets with an aspect ratio $R/\Delta R < 100$, values $\varepsilon_0 \approx 0.15$ J/ng and $\bar{v} \approx 0.7 \cdot 10^7$ cm/s, and also to record a neutron yield on the order of $N_{DT} \approx 10^3$. On the other hand, in the experiments with targets having $R/\Delta R = 100$–300, proposed to increase the specific energy input and the shell travel time[3] and carried out for the first time with the "SOKOL" facility,[3,16] exhibited the same properties as those with $R/\Delta R < 100$, the only difference being that the measured collapse times were as a rule longer than the calculated ones.[13] This discrepancy can be attributed to the fact that the acceleration of thin shells ($R/\Delta R > 100$) deviates substantially from spherical symmetry at the illumination inhomogeneities $\gamma \approx 20$–40% realized in experiment,[27] and to the target-thickness variation

$$\delta_t = 2 \frac{\Delta R_{max} - \Delta R_{min}}{\Delta R_{max} + \Delta R_{min}} \approx 1\text{–}5\%.$$

Values $\varepsilon_0 \approx 0.25$ J/ng and $\bar{v} \approx 10^7$ cm/s were reached in experiments with $R/\Delta R \approx 200$.

3. INVESTIGATION OF GASDYNAMIC PARAMETERS OF IRRADIATED TARGETS

The laser energy needed to reach a specified multiplication coefficient Y depends substantially on the degree of compression δ of the thermonuclear fuel, on the absorption efficiency ε_a, and on the hydrodynamic energy-transfer coefficient η_h of the compressed part of the target. It is easy to

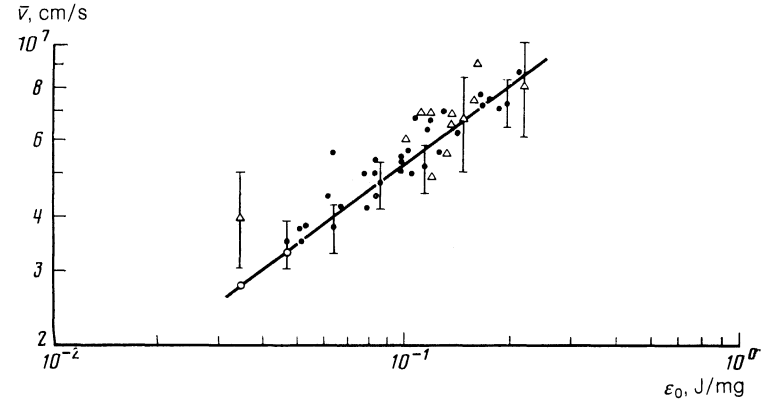

FIG. 4. Dependence of average velocity of shell travel towards the center on the specific energy input: ●—corona, △—"TXD," ○—calculation.

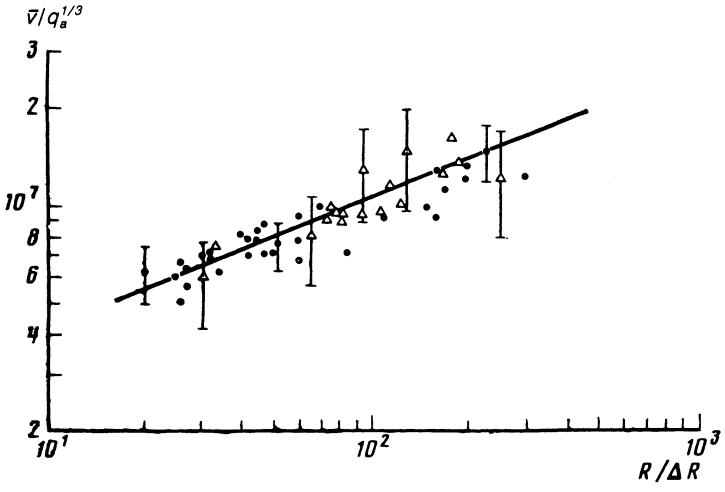

FIG. 5. Reduced average shell travel velocity $\bar{v}/q_a$ towards the target vs the target aspect ratio; $[v] = 10^7$ cm/s, $[q] = 10^{14}$ W/cm^2; ●—corona; △—"TXD."

show that under the simplest assumptions the dependence of E_L on δ, ε_a, and η_h is given by

$$E_L \infty \delta^{-2} Y^3 \varepsilon^{-4} f(T_i), \quad \varepsilon \infty \varepsilon_a \eta_h. \tag{6}$$

This expression will undoubtedly not lead to numerical estimates of E_L (this would call for gasdynamic calculations), but will describe lucidly the physical dependence of the laser energy on the considered parameters. The absorptivity for Nd-laser systems with $\lambda \approx 1.06$ μm is $\varepsilon_a \approx 0.2$–$0.3$, whereas the hydrodynamic efficiency and the mass coefficient are respectively $\eta_h \approx 0.05$–0.1 and $\eta_m \approx 0.3$ (Refs. 1, 2, 11). In view of such low values of the effectiveness and of the hydrodynamic efficiency, high laser energies E_L ($Y = 1$) $\approx$ 100–300 kJ are needed to obtain a thermonuclear explosion.[2] This calls for great efforts to develop high-power short-wave lasers (conversion of the laser radiation into the harmonics $2\omega_0$, $3\omega_0$, $4\omega_0$, Ref. 15; excimer lasers with $\lambda \approx 0.25$ μm, Ref. 29). This trend towards the development of laser systems for thermonuclear fusion entails increasing the effectiveness of the classical absorption $\varepsilon_a \propto \lambda^{-2}$ and suppression of the nonclassical interactions ($\propto q\lambda^2$) when lowering the wavelength of the heating radiation. In addition, owing to penetration of the laser radiation into denser plasma regions, the mass-flow rate $\dot{m}$, the ablation pressure P_a, and the hydrodynamic efficiency also increase in this case, reducing in final analysis the required laser energy. The promise offered by this trend is also the cause of considerable interest in experimental investigations of the indicated parameters.

The ablation pressure, the mass-flow rate, the hydrodynamic efficiency, and the mass coefficient were measured in the present experiment by recording the energy distribution of the laser-plasma ions by the "Ions" procedure.[12] According to Refs. 30–32, the values of $\dot{m}$ and $\bar{P}_a$ are

$$\dot{m} = \frac{2E_{\text{п}}}{\bar{v}_i^2 4\pi \bar{R}_{\text{cr}}^2 \tau_p}, \quad \bar{P}_{\text{a}} = \gamma \dot{m} \bar{v}_i, \tag{7}$$

where $\bar{v}_i$ is the average plasma-ion scatter velocity, and $\gamma \approx 0.35$ in the range $q_a \approx 10^{12}$–10^{14} W/cm^2. The dependences of $\bar{v}_i$, $\dot{m}$, and $\bar{P}_a$ on the absorbed laser energy flux density q_a in experiments with the "SOKOL" facility are shown in Figs. 6, 7, and 8, respectively. The figures show also the results obtained with other laser facilities.[30–34] Our present results are well interpolated by the relations

$$\bar{v}_i \approx 6 \cdot 10^7 q_{\text{cr}}^{0.23} \text{ cm/s}, \quad \dot{m} \approx 7.1 \cdot 10^5 q_{\text{cr}}^{0.9} \text{ g/cm}^2 \cdot \text{s},$$
$$\bar{P}_a \approx 14.6 q_a^{1.1} \text{ Mbar}, \quad [q_a] = 10^{14} \text{ W/cm}^2, \tag{8}$$

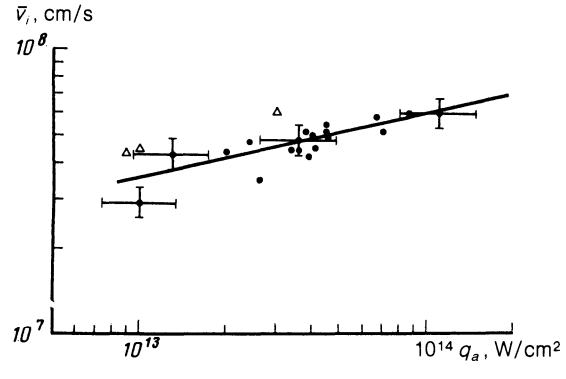

FIG. 6. Average plasma expansion velocity vs the absorbed laser-energy flux density: ●—"SOKOL," △—"Vulcan," Rutherford Lab.[30,31]

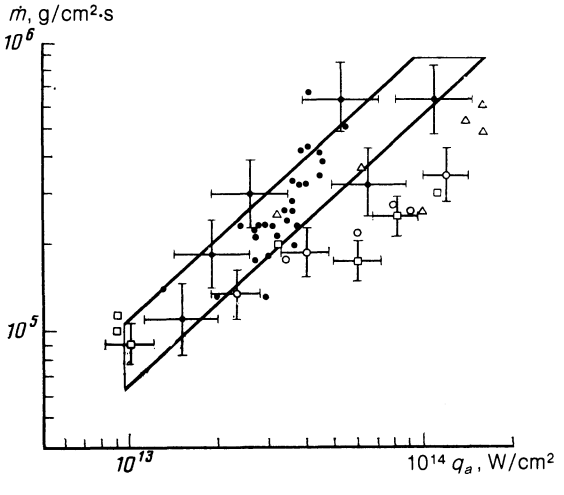

FIG. 7. Mass flow rate vs absorbed laser-energy flux density: ●—"SOKOL," □—"Vulcan," Rutherford Lab.,[30,31] ○—"Chroma-I," KMS Fusion,[33,34] △—"Omega," LLE.[32]

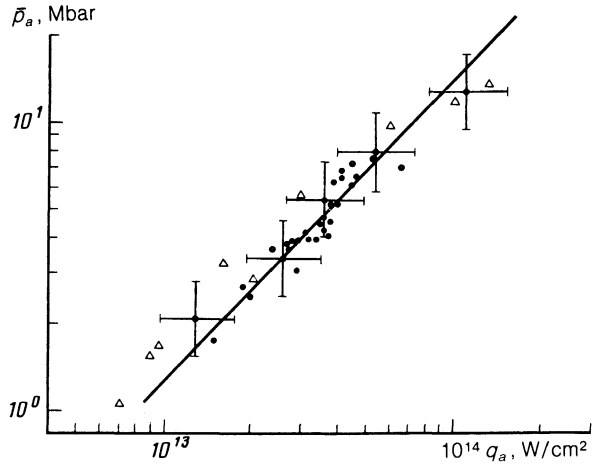

FIG. 8. Average ablation pressure vs the absorbed laser-energy flux density: ●—"SOKOL"; △—"Vulcan," Rutherford Lab.[30,31]

agree with results of Refs. 30–34, and are in accord with the theoretical models.

Next, the "Ions" procedure in experiments with targets having $R/\Delta R = 30$–80 registered as a rule a two-spike structure of the current to the ion-collectors (see Fig. 9). The reason for this structure is that the target corona is more heated than its compressed part. Thus, in the experiments considered, the temperature of the compressed glass was approximately 5–10 times lower than the maximum electron temperature of the corona. This led to separation of the evaporated part from the compressed one following expansion to appreciable (>10 cm) distances, and made it possible to measure the mass and energy of the compressed part of the target, and determine the hydrodynamic efficiency and the mass coefficient. Table I lists the measured values of η_t and η_h, as well as the mass flow rate and ablation pressure estimated on the basis of simple physical relations in which the measured η_t and η_h are used:

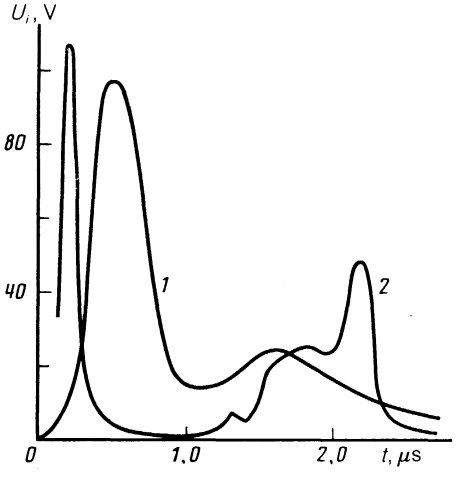

FIG. 9. Time dependence of ion current $i(t)$ to the collector in experiment No. 45 at $2R_t \approx 107$ μm, $\Delta R \approx 1.7$ μm, $P_{DT} \approx 5$ atm, $\tau_p \approx 1.2$ ns, $E_a \approx 8.5$ J, and $q \approx 3.0 \cdot 10^{14}$ W/cm². 1—Experiment, $U_i(t) = i(t)R$, $R \approx 72$ Ω, $L \approx 11.0$ cm is the distance from the target to the collector $\Omega \approx 3.3 \cdot 10^{-4}$ rad is the solid angle of the collector; 2—calculation.

$$\dot{m} = \frac{(1-\eta_M)M_0}{4\pi \bar{R}_{cr}^2 \tau_a}, \quad \bar{P}_a = 3\frac{\Delta R}{R}\rho\eta_r\varepsilon_0,$$
$$\tau_a = \tau_p, \quad \tau_p \leqslant \tau_*, \quad \tau_a = \tau_*, \quad \tau_p \geqslant \tau_*. \tag{9}$$

The table lists also the values of $\dot{m}$ and $\bar{P}_a$ measured in accordance with Refs. 30–32 (see Figs. 7 and 8). As seen from the table, the hydrodynamic energy-transfer coefficient and the mass coefficient depend on the specific energy input. With increase of the latter, the mass coefficient decreases (the evaporated part of the target increases), and the hydrodynamic efficiency increases. Such a dependence is typical of these gasdynamic parameters.[1,25]

It must be noted here that the straight lines in Figs. 6, 7, and 8 were drawn through the experimental points by least squares and correspond to relations (8). The strip in Fig. 7 is the error corridor of the measured $\dot{m}$. The measurement errors of $\dot{m}$ and $\bar{P}_a$ are given in the table and are the sums of the measurement errors of E_a, v_i, and $\bar{R}_{cr}$. On the other hand, the errors of the parameters η_h and η_t are the sums of the measurement errors of the ion currents $i(t)$ and velocities v_i, of the initial target mass ($\Delta M_0/M_0 \approx 0.01$), and of the deviations of the effective ion charge Z_{eff} in the evaporated and compressed regions of the target from Z_{eff}. In the experiments described, $|Z_{eff} - \bar{Z}_{eff}|/Z_{eff}$ amounts to ≈ 0.1–0.2, while $\Delta\eta_h/\eta_h \approx 0.3$ and $\Delta\eta_t/\eta_t \approx 0.3$. The procedure of determining $\bar{Z}_{eff}$ from collector measurements is described in detail in Ref. 12.

In experiments with targets having aspect ratios $R/\Delta R > 100$, however, no two-spike ion-current structure is observed as a rule. This is explained by gasdynamic calculations which yield an increase of the hydrodynamic efficiency to approximately 0.2 and an increase of the evaporated target mass to ≈ 0.8 for targets with high aspect ratio at $\varepsilon_0 \approx 0.2$–$0.3$ J/ng. As a result, the specific energy releases in the evaporated and compressed parts of the target become approximately equal. Thus, a second ion-current spike was observed only in experiments 50 and 65, in which the specific energy input was the lowest.

Thus, the mass flow rate and the ablation pressure at the maximum absorbed laser-energy flux density $q_a \approx 10^{14}$ W/cm² reached in the experiments with the "SOKOL" facility are respectively $\dot{m} \approx 6 \cdot 10^5$ g/cm²·s and $P_a \approx 13$ mbar. In experiments with targets having an aspect ratio $R/\Delta R = 30$–80, the hydrodynamic efficiency and the mass coefficient are $\eta_h \approx 0.05$–0.1 and $\eta_t \approx 0.4$–0.2 at $\varepsilon_0 \approx 0.1$ J/ng. In the case of large aspect ratios $R/\Delta R = 100$–300 we have $\eta_h \approx 0.8$–0.1 and $\eta_t \approx 0.25$–0.3 at $\varepsilon_0 \approx 0.12 = 0.14$ J/ng.

4. INVESTIGATION OF LIMITATION OF ELECTRON HEAT CONDUCTION IN A LASER PLASMA

It is precisely the electron heat conduction which is the principal mechanism of heat transfer from the laser-energy absorption region to the dense regions of the target. At laser-radiation energy-flux densities $q\lambda^2 \gtrsim 10^{15}$ W/cm²·μm², a substantial role is played by the confinement of the electronic heat flow. In gasdynamic calculations this effect is described as follows:

$$q_e^{-1} = |q_{ec}|^{-1} + q_{em}^{-1},$$

where q_e is the absolute value of the energy-flux density carried by the thermal electrons, $q_{ec} = -\varkappa_e \nabla T_e$ is the classi-

TABLE I.

	Experiment No.							Errors
	45	56	60	61	63	64	65	
$2R_t$, μm	106.9	142.6	92.5	107.4	114	106.6	129.8	–
ΔR, μm	1.7	0.28	1.52	1.2	0.8	0.9	0.58	–
$R/\Delta R$	31	255	30	45	70	59	112	–
M_0, ng	150	45	100	107	84	80	77	
$2R_{cr}$, μm	–	143	106	120	134	84	130	$\Delta R_{cr} \approx \pm 10\,\mu$m
τ_p, ns	1.2	0.3	0.3	1.0	1.0	1.0	1.0	$\Delta\tau \approx \pm 0.05$ ns
τ_*, ns	$\tau_* > \tau_p$	1.05	0.96	1.0	0.93	0.75	1.1	$\Delta\tau \approx \pm 0.1$ ns
$\bar{v}$, cm/s	–	$0.7 \cdot 10^7$	$0.5 \cdot 10^7$	$0.6 \cdot 10^7$	$0.6 \cdot 10^7$	$0.7 \cdot 10^7$	$0.5 \cdot 10^7$	$\Delta\bar{v}/\bar{v} \approx 0.1$
q_a, W/cm^2	–	$2.7 \cdot 10^{13}$	$1.1 \cdot 10^{14}$	$2.9 \cdot 10^{13}$	$2.7 \cdot 10^{13}$	$5.4 \cdot 10^{13}$	$2.0 \cdot 10^{13}$	$\Delta q_p/q_p \approx 0.35$
ε_0, J/ng	0.06	0.12	0.12	0.1	0.14	0.11	0.14	$\Delta E_p/E_p \approx 0.2 \pm 0.25$
η_t	0.5	0.25	0.25	0.35	0.4	0.2	0.3	
η_h	0.03	0.08	0.06	0.1	0.05	0.06	0.1	–
$\dot{m}$, g/cm^2·s	–	$2.2 \cdot 10^5$	$6.2 \cdot 10^5$	$2.2 \cdot 10^5$	$0.7 \cdot 10^5$	$4.8 \cdot 10^5$	$1.2 \cdot 10^5$	$\Delta\dot{m}/\dot{m} \approx 0.25$
$\bar{P}_a$, Mbar	–	3.8	13.0	2.6	2,1	8.0	2.5	$\Delta\bar{P}_a/\bar{P}_a \approx 0.35$
$\dot{m}$ (Ref. 9)	–	$1.7 \cdot 10^5$	$7.4 \cdot 10^5$	$1.5 \cdot 10^5$	$0.9 \cdot 10^5$	$2.8 \cdot 10^5$	10^5	
$\bar{P}_a$ (Ref. 9)	–	2.8	29	17	7.4	9.6	9.2	

cal flux density, $q_{em} = f n_e T_e (T_e/m_e)^{1/2}$ is the electronic heat-flux limit, and f is the confinement coefficient. The latter is estimated in theoretical papers[35] at $(zm_e/m_i)^{1/2} \leqslant f \leqslant (zm_e/m_i)^{1/4}$, or $10^{-2} \leqslant f \leqslant 10^{-1}$. Strong confinement of the electron heat conduction take place in experiments with high flux values $q\lambda^2 \gtrsim 10^{15}$ W/cm$^2 \cdot \mu$m^{-2}, to which small $f \sim 10^{-2}$ correspond.[30,36] Since the most promising for laser-driven thermonuclear fusion is the flux density range $10^{13} \leqslant q\lambda^2 \leqslant 10^{15}$ W/cm$^2 \cdot \mu$m^{-2}, where adiabatic compression of the thermonuclear fuel is in fact possible, it is precisely in this range that importance attaches to detailed investigations of the limitation of the electronic heat conduction.

These investigations are based on a comparison of the measured laser-plasma parameters that are most sensitive to the value of the electronic heat flux with the results of gasdynamic calculations carried out at different values of the limitation coefficient.[30–34,36,37] This coefficient was determined in Ref. 37 by comparing the experimental multiply-charged silicon-ion x-ray yields recorded in experiment No. 38 with the "SOKOL" facility at $q \approx 2.1 \cdot 10^{14}$ W/cm^2 and $q_a \approx 4 \cdot 10^{14}$ W/cm^2. The best agreement between calculation and experiment is observed for weak confinement of the electron heat conduction $f \approx 0.2$–0.6.

We have compared in the present study the experimental values of the laser-energy absorption coefficient, and of the target collapse, measured by the "Shock-wave" and "Corona" methods, likewise in experiment No. 38, with the results of numerical calculations in accordance with the "ZARYA" program, for the recorded value of the laser energy incident on the target and for different values of the confinement coefficient. The results are shown in Fig. 10 and, just as in Ref. 37, favor a weak confinement $f > 0.1$–0.2. The experimental data agree best with the calculations at $f \approx 0.3$–0.4. In addition, the good agreement between the experimental $R_{cr}(t)$ dependences and the values of the collapse time, for a run of experiments with $R/\Delta R = 30$–80 and the calculated values obtained under the assumption $f = 0.2$–0.4 also favor a weak confinement of the electronic heat conduction.

The foregoing analysis provides thus more detailed data on the value of the electron heat flux in experiments with the "SOKOL" facility, and permits calibration of the values of the limitation coefficient for $q \approx 2.0 \cdot 10^{14}$ and $q_a \approx 0.4 \cdot 10^{14}$ W/cm^2. It would be useful to obtain in the future more detailed values of the coefficient f in the entire flux-density range of interest and determine the dependence of the limitation on the incident or absorbed laser-energy flux.

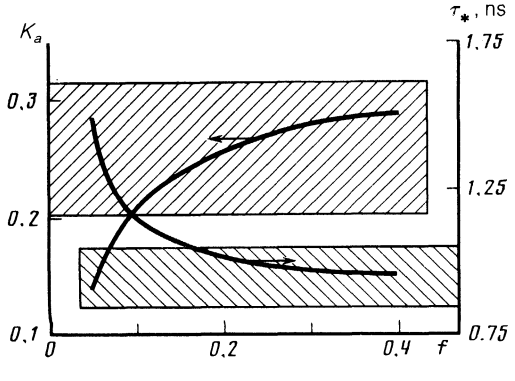

FIG. 10. Calculated dependences of the absorption coefficient K_a and the target collapse time on the electronic heat conduction confinement coefficient (experiment No. 38). The experimental data are represented by the shaded strips.

CONCLUSION

We developed, through experiments with the "SOKOL" facility, methods for measuring the gasdynamic parameters of irradiated targets. We investigated the dynamics of compression of gas-filled glass microspheres with aspect ratios $R/\Delta R = 30$–300. We investigated the dependences of the average time of shell travel to the center on the aspect ratio and on the specific energy input at the instant of target collapse, in the range $\varepsilon_0 \approx 0.03$–$0.25$ J/ng. On the basis of the relations obtained and of the dependences of the laser-energy absorption coefficient on the flux density[11] we optimized the parameters of the laser + target system, using as a criterion the increase of the specific energy input when the laser-pulse duration is matched to the target collapse time. Thus, experiments on targets having an aspect ratio $R/\Delta R = 30$–80 yielded a specific energy input $\varepsilon_0 \approx 0.15$ J/ng, an average target travel velocity $\bar{v} \approx 0.7 \cdot 10^7$ cm/s, and a neutron yield on the order of $N_{DT} \sim 10^3$. On the other hand, values $\varepsilon_0 \approx 0.25$ J/ng and $\bar{v} \approx 10^7$ cm/s were reached in experiments with $R/\Delta R \approx 200$.

We investigated the dependences of the average dispersal velocity of the laser plasma, the mass flow rate, and the average ablation pressure as functions of the absorbed laser-energy flux density in the range $q_a \approx (0.1$–$1.0) \cdot 10^{14}$ W/cm^2. At the maximum attained values $q_a \approx 10^{14}$ W/cm^2 in the experiments with the "SOKOL" facility, the mass flow velocity and the ablation pressure are $\dot{m} \approx 6 \cdot 10^5$ g/cm$^2 \cdot$s and $P_a \approx 13$ Mbar. Measurements of the coefficient of hydrodynamic energy transfer of the compressed part of the target and of the mass coefficient have shown that the hydrodynamic efficiency and the evaporated fraction of the target increase with increase of the specific energy input. In experiments with targets having $R/\Delta R = 100$–300 the results are $\eta_h \approx 0.5$–0.1 and $\eta_t \approx 0.4$–0.2 at 0.1 J/ng. For $R/\Delta R = 100$–300, on the other hand, $\eta_h \approx 0.08$–0.1 and $\eta_t \approx 0.25$–0.3 at $\varepsilon_0 \approx 0.12$–$0.14$ J/ng.

To calibrate the limitation coefficient of the electron heat conduction, the measured parameters that are most sensitive to the electron heat flux were compared simultaneously with the results of gasdynamic calculations by the "ZARYA" program for different values of the confinement coefficient. It was found that under the "SOKOL" experimental conditions the values $q \approx 2.0 \cdot 10^{14}$ W/cm^2 and $q_a \approx 0.4 \cdot 10^{14}$ W/cm^2 correspond to weak confinement of the electron heat flux, $f \approx 0.3$–0.4.

[1] N. G. Basov, Yu. A. Zakharenkov, N. N. Zorev *et al.*, Heating and compression of laser-irradiated thermonuclear targets. Itogi Nauki i Tekhniki, Vol. 26, VINITI, 1982.
[2] N. G. Basov, Yu. A. Mikhaĭlov, G. V. Sklizhov, and S. I. Fedotov, Laser-driven thermonuclear facilities. *ibid.* Vo. 25, VINITI, 1984.
[3] V. V. Volenko, A. F. Ivanov, L. A. Myalitsin *et al.*, Pis'ma Zh. Eksp. Teor. Fiz. **37**, 328 (1983) [JETP Lett. **37**, 389 (1983)].
[4] E. N. Avrorin, V. A. Eroshenko, I. A. Zaretskiĭ *et al.*, Zh. Eksp. Teor. Fiz. **87**, 417 (1984) [Sov. Phys. JETP **60**, 239 (1984)].
[5] V. V. Volenko, A. I. Zuev, A. F. Ivanov *et al.*, Proc. 3rd All-Union "Laser Optics" Conf., Leningrad, 4–8 Jan. 1982.
[6] I. A. Abramov, V. V. Volenko, N. P. Voloshin *et al.*, Zh. Eksp. Teor. Fiz. **83**, 988 (1982) [Sov. Phys. JETP **56**, 557 (1982)].

[7]V. V. Volenko, A. F. Ivanov, L. A. Myalitsin *et al.*, Prib. Tekh. Eksp. No. 1, 170 (1985).
[8]E. K. Strom, H. G. Ahlstrom, M. J. Boyle *et al.*, Phys. Rev. Lett. **40**, 1570 (1978).
[9]N. G. Basov, P. P. Volosevich, E. G. Gamalii *et al.*, Zh. Eksp. Teor. Fiz. **78**, 420 (1980) [Sov. Phys. JETP **51**, 212 (1980)].
[10]C. E. Max, C. F. McKee, and W. C. Mead, Phys. Fluids **23**, 1620 (1980).
[11]Yu. A. Zysin, I. A. Abramov, V. V. Volenko *et al.*, Zh. Eksp. Teor. Fiz. **83**, 1346 (1982) [Sov. Phys. JETP **56**, 773 (1982)].
[12]V. V. Volenko, A. L. Zapysov, A. I. Zuev *et al.*, Kvant. Elektron. (Moscow) **11**, 44 (1984) [Sov. J. Quant. Electron. **14**, 26 (1984)].
[13]V. V. Volenko, A. L. Zapysov, A. I. Zuev *et al.*, *ibid.* p. 1179 [795].
[14]A. S. Ganeev, A. L. Zapysov, I. M. Izrailev *et al.*, Prib. Tekh. Eksp. No. 3, 188 (1982)].
[15]J. L. Emmett, W. F. Krupke, and J. B. Trenholme, Kvant. Elektron. (Moscow) **10**, 5 (1983) [Sov. J. Quant. Electron. **13**, 1 (1983)].
[16]V. V. Volenko, A. I. Zuev, A. F. Ivanov *et al.*, *ibid.* p. 2350 [1529].
[17]A. S. Ganeev, A. L. Zapysov, A. L. Izrailev *et al.*, *ibid.* **7**, 2227 (1980) [**10**, 1294 (1980)].
[18]N. M. Barysheva, A. I. Zuev, N. G. Karlykhanov *et al.*, Zh. Vych. Mat. Mat. Fiz. **22**, 401 (1982)].
[19]Yu. V. Afanas'ev, N. G. Basov, O. N. Krokhin *et al.*, Interaction of high-power laser radiation with plasma. Itogi Nauki i Tekhniki, Vol. 17, VINITI, 1978.
[20]C. E. Max and C. F. McKee, Phys. Rev. Lett. **39**, 1336 (1977).
[21]K. A. Brueckner and R. S. Janda, Nucl. Fusion **17**, 451 (1977).
[22]K. A. Brueckner, *ibid.* **16**, 387 (1976).
[23]E. N. Avrorin, Fiz. Plazmy **7**, 694 (1981) [Sov. J. Plasma Phys. **7**, 381 (1981)].
[24]M. H. Key, M. J. Lamb, C. L. S. Lewis *et al.*, Appl. Phys. Lett. **34**, 550 (1979).
[25]Yu. A. Zakharenkov, G. V. Sklizkov, and A. S. Shikanov, Kvant. Elektron. (Moscow) **10**, 1679 (1983) [Sov. J. Quant. Electron. **13**, 1205 (1983)].
[26]S. A. Litzring, E. J. Thorsos, W. D. Friedman *et al.*, J. Appl. Phys. **54**, 6302 (1983).
[27]V. V. Volenko and V. B. Kryuchenkov, Kvant. Elektron. (Moscow) **6**, 1343 (1979) [Sov. J. Quant. Electron. **9**, 789 (1979)].
[28]E. N. Avrorin, A. N. Zuev, N. G. Karlykhanov *et al.*, Pis'ma Zh. Eksp. Teor. Fiz. **32**, 457 (1980) [JETP Lett. **32**, 437 (1980)].
[29]Excimer Lasers, Ch. K. Rhoades, ed., Springer, 1979.
[30]J. Goldsack, J. D. Kilkenny, B. J. MacGowan *et al.*, Phys. Fluids **25**, 1634 (1982).
[31]A. Hauer, W. C. Mead, O. Willi *et al.*, Phys. Rev. Lett. **53**, 256 (1984).
[32]B. Yaakobi, J. Delettrez, L. M. Goldman *et al.*, Phys. Fluids **27**, 516 (1984).
[33]J. A. Tarvin, W. B. Fechner, J. T. Larsen *et al.*, Phys. Rev. Lett. **51**, 1355 (1983).
[34]W. B. Fechner, C. L. Shepard, G. E. Busch *et al.*, Phys. Fluids **27**, 1552 (1984).
[35]J. Lindle, Nucl. Fusion **14**, 522 (1974).
[36]W. C. Mead, E. M. Campbell, W. L. Kruer *et al.*, Phys. Fluids **27**, 1301 (1984).
[37]V. V. Volenko, A. L. Zapysov, A. I. Zuev *et al.*, Kvant. Elektron. (Moscow) **10**, 1281 (1983) [Sov. J. Quant. Electron. **13**, 828 (1983)].

Translated by J. G. Adashko